ARTICLE

Imaging the Operation of a Carbon Nanotube Charge Sensor at the Nanoscale

David Brunel,[†] Alexandre Mayer,[‡] and Thierry Mélin[†,*]

[†]Institut d'Electronique, de Microélectronique et de Nanotechnologie, CNRS UMR 8520, Avenue Poincaré, F-59652 Villeneuve d'Ascq, France, and [‡]Laboratoire de Physique du Solide, Facultés Universitaires Notre-Dame de la Paix, 61 Rue de Bruxelles, B-5000 Namur, Belgique

ABSTRACT Carbon nanotube field effect transistors (CNTFETs) are of great interest for nanoelectronics applications such as nonvolatile memory elements (NVMEs) or charge sensors. In this work, we use a scanning-probe approach based on a local charge perturbation of CNTFET-based NVMEs and investigate their fundamental operation from combined transport, electrostatic scanning probe techniques and atomistic simulations. We experimentally demonstrate operating devices with threshold voltages shifts opposite to conventional gating and with almost unchanged hysteresis. The former effect is quantitatively understood as the emission of a delocalized image charge pattern in the nanotube environment, in response to local charge storage, while the latter effect points out the dominant dipolar nature of hysteresis in CNTFETs. We propose a simple model for charge sensing using CNTFETs, based on the redistribution of the nanotube image charges. This model could be extended to gas or biosensing, for example.

KEYWORDS: carbon nanotube · field effect transistor · electrostatic force microscopy · Kelvin probe microscopy · charge injection · charge detection

Nonvolatile memory elements (NVMEs) are essential for nanoelectronics applications and may combine silicon and carbon technologies[1] to enhance charge storage[2,3] and charge detection capabilities.[4−7] NVMEs built on dielectrics[8,9] or ferroelectrics[10] have been demonstrated from the hysteresis[11−13] of carbon nanotube field effect transistors (CNTFETs). Most devices are based on the intentional generation of a pronounced hysteresis in the device transfer characteristics by a high gate biasing of the CNTFET ("WRITE" step), and on the subsequent detection of the change in the transistor source-drain current ("READ" step). The generation of the hysteresis—and thus the operation principle of the device—had been assigned as an injection of charges from the nanotube into the gate dielectric layer upon high gate biasing. In this Article, we investigate the fundamental operation mechanisms of CNTFET-based NVMEs at the nanoscale. We use a scanning-probe approach based on a *local* charge perturbation of CNTFET-based NVMEs in the plane of the device. This allows the NVMEs to be investigated jointly from transport and electrostatic scanning-probe microscopy,[14,15] here electrostatic force microscopy (EFM) and Kelvin force microscopy (KFM), so as to map local charges and surface potentials, and to understand their operation in link with atomistic electrostatic simulations. We demonstrate experimentally operating devices with threshold voltage shifts opposite to conventional gating and mostly unchanged hysteresis.[8−10] The device operation is quantitatively understood as the emission of a delocalized image charge pattern in the nanotube environment, in response to local charge storage.

*Address correspondence to thierry.melin@isen.iemn.univ-lille1.fr.

Received for review June 2, 2010 and accepted September 15, 2010.

Published online September 24, 2010. 10.1021/nn1012435

RESULTS AND DISCUSSION

The CNTFET used here consists of a single-walled carbon nanotube transistor fabricated on a 320 nm thick SiO_2 layer. To achieve a local WRITE step on the CNTFET (see illustration in Figure 1), we use a scanning-probe tip polarized at V_{inj} and brought into contact (with a few nN force) onto the oxide layer close to the nanotube ($\simeq$150 nm), while grounding the transistor backgate, source, and drain ($V_G = V_S = V_D = 0$, see Figure 1b). This creates a local charge perturbation Q_{inj} in the vicinity of the CNTFET channel (see Experimental Methods). The position of Q_{inj} with respect to the nanotube can be visualized by the persistent charge spot Q_{stored} which is left into the SiO_2 layer supporting the nanotube after the charge injection experiment, with $Q_{stored} = \alpha Q_{inj}$ ($\alpha < 1$). After the charge injection, the device is investigated from its transport characteristics (Figure 1a) and imaged by EFM and KFM (see Experimental Methods and the illustration in Figure 1c).

The influence of the local WRITE step on the CNTFET electrical properties is pre-

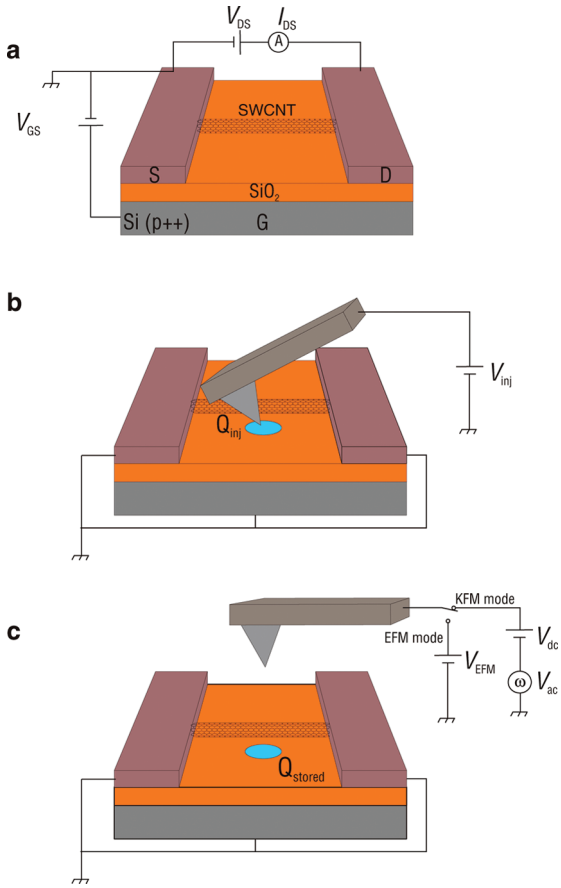

Figure 1. CNTFET configuration, charge storage, and imaging. (a) The nanotube is deposited on a 320 nm thick thermal SiO_2 layer and contacted with palladium leads. The CNTFET is characterized by recording the drain−source current I_{DS} as a function of the backgate bias V_G, at fixed source drain bias (here $V_{DS} = -1$ V). (b) Schematics of the local in-plane charge injection experiment, in which the atomic force microscopy tip is brought in static contact with the SiO_2 and biased at an injection voltage V_{inj} (here $V_D = V_S = V_G = 0$) to transfer a local charge (up to a few tens of elementary charges) to the SiO_2 surface in the vicinity of the CNTFET channel. (c) Scanning probe experiments, in which the CNTFET is unbiased ($V_D = V_S = V_G = 0$) and the tip is either mechanically actuated and polarized at V_{EFM} (EFM mode), or electrostatically actuated using an excitation bias $V_{dc} + V_{ac}\cos(\omega t)$ (KFM mode). EFM and KFM modes enable the measurement of electrostatic force gradients and local surface potentials, respectively.

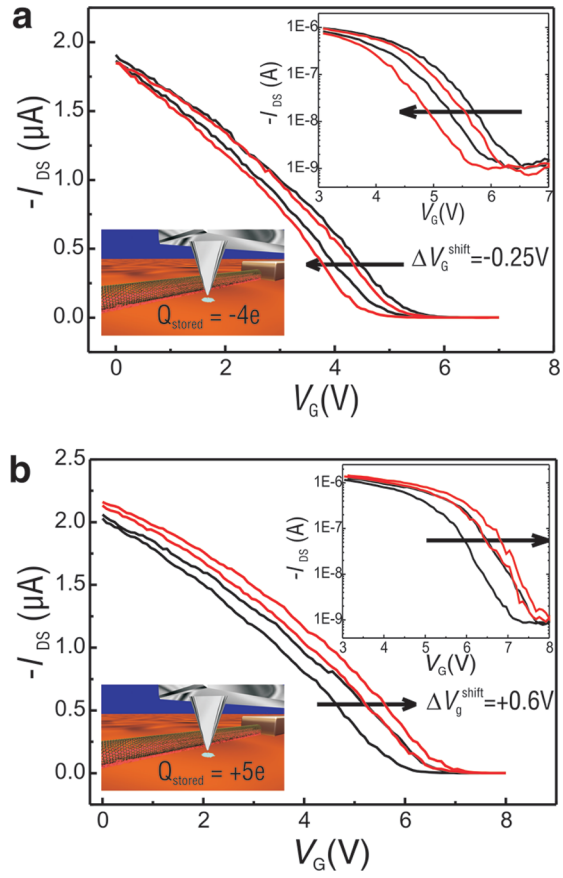

Figure 2. Electrical response to a local charge perturbation. (a) CNTFET transfer characteristics I_{SD} (V_{DS}) in linear scale (mainframe) and in logarithmic scale (inset) before (black curve) and after (red curve) a local negative charge injection, $Q_{stored} = -4e$, located at 180 nm from the CNTFET channel (the 3D inset is out of scale). The transfer characteristics shift toward negative gate bias showing that the nanotube is sensitive to a positive effective gating. (b) Same plot, for a positive charge injection, $Q_{stored} = +5e$, located at 140 nm from the CNTFET channel. The transfer characteristics shift toward positive gate bias shows that the nanotube is sensitive to a negative effective charge gating.

sented in Figure 2, first for a negative charge injection ($V_{inj} = -6$ V, top), and then for a positive charge injection of ($V_{inj} = +6$ V, bottom). The charge injections were achieved, respectively, at a distance of 180 and 140 nm from the CNTFET channel. As seen from Figure 2, two important observations can be made from the evolution of the CNTFET transfer characteristics upon charge injection: (i) Unlike previous CNTFET-based NVMEs,[8−10] the width of the hysteresis loop is only weakly affected by the local WRITE step. Transfer characteristics exhibit rather a global shift $\Delta V_{G,shift}$ as a function of the gate bias, which can exceed the device hysteresis width. (ii) Strikingly, the sign of the gate voltage shift $\Delta V_{G,shift}$ is opposite to a conventional gating process.[5] This is obvious from Figure 2a ($\Delta V_{G,shift} = -0.25$ V), in which the CNTFET current decreases at fixed gate bias after the negative charge injection ($V_{inj} = -6$ V). A negative charge gating would enhance the source−drain current for such a p-type CNTFET and induce rather a positive $\Delta V_{G,shift}$. This behavior is confirmed by the positive charge injection ($V_{inj} = +6$ V) from Figure 2b in which $\Delta V_{G,shift} = +0.6$ V: the CNTFET current increases at fixed gate bias after charge injection, in contrast with the behavior expected from a positive gating.

To identify the fundamental mechanisms governing such a nanoscale NVME, we use scanning probe techniques to map the electrostatic properties of the device. EFM images (color scale 3 Hz) and KFM images (color scale 200 mV) of the device before charge injection are shown in Figure 3 panels b and c, respectively, and offer a nanoscale view of the device charge and surface potential distribution, respectively. They show the

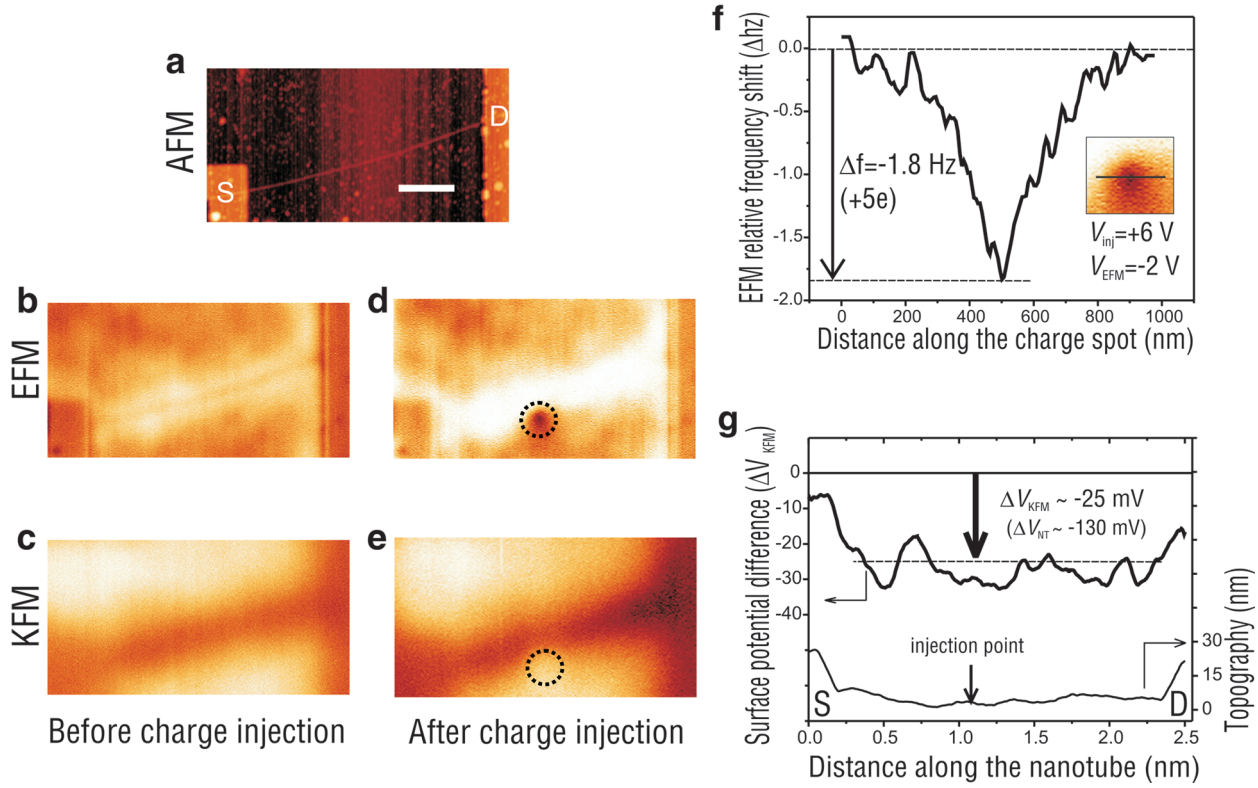

Figure 3. EFM and KFM imaging: (a) CNTFET topography image (scale bar: 600 nm). (b) EFM and (c) KFM image of the device before charge injection; (d and e) same images after local positive charge injection. The local charge spot is both visible in the EFM image (dark spot) and in the KFM image (bright surface potential spot). A cross section of the EFM signal across the injection spot is shown in panel f. A delocalized charge is visible along the nanotube after the local charge injection, as seen from (d) EFM (2.5 Hz scale) and (e) KFM (200 mV scale) images. The difference of the KFM signals ($\Delta V_{KFM} = -25$ mV) along the nanotube between panels e and c is shown in panel g, corresponding to a shift $\Delta V_{NT} = -130$ mV of the nanotube electrostatic potential (see text).

electrostatic landscape along the device channel prior to its operation, either mapped from electrostatic force gradients (EFM) or from surface potentials (KFM). The same images have been acquired after the positive charge injection ($V_{inj} = +6$ V), and are shown in Figure 3d,e. They reveal the positive charge injection spot Q_{stored} (positive surface potential feature in Figure 3e), here located 140 nm away from the nanotube, for which a cross section of the EFM signal is presented in Figure 3f. The EFM signal cross-section (here a frequency shift of -1.8 Hz) is used to extract the amount of charge injected into the oxide,[16] and provides $Q_{stored} = +5e$. The accuracy of frequency shift measurements is better than 15%. Both EFM and KFM images (Figure 3d,e) after charge injection reveal a drastic change in the CNTFET channel electrostatic landscape, corresponding to a brighter nanotube EFM signal in Figure 3d and to a darker contrast of the nanotube in the surface potential KFM image of Figure 3e. This demonstrates the presence of a delocalized negative charge Q_{NT} along the nanotube, likely stored at the SiO_2/nanotube interface as in the case of direct charge injection experiments into nanotubes.[14] This crucial observation is in agreement with the NVME transport characteristics (Figure 2b) showing an opposite gating as compared to the charge injection process and suggests that the NVME behavior (READ step) is dominated by the modification in the CNTFET channel electrostatic environment, that is, here the delocalized charge Q_{NT} along the nanotube. The shift of the nanotube surface potential due to the injection process (difference in the KFM signals along the nanotube in Figure 3e,c) is shown in Figure 3g. It is almost constant and equals $\Delta V_{KFM} = -25$ mV. This quantity however only corresponds to a fraction of the nanotube electrostatic potential shift, due to side-capacitance averaging effects between the KFM probe and the sample.[17] The actual value of the nanotube electrostatic potential shift is extracted quantitatively, using a calibration procedure of KFM signals in the case of CNTFETs,[15] and equals $\Delta V_{NT} = -130$ mV.

Figure 4 presents a summary of four independent charge injection experiments conducted on two different NVMEs,[18] both investigated by combined transport and scanning-probe measurements. We first plotted in Figure 4a the nanotube electrostatic potential ΔV_{NT} (as quantitatively determined from KFM experiments) as a function of the gate voltage shift $\Delta V_{G,shift}$ of the CNTFET. The linear behavior with negative slope shows that the NVME mostly reacts to the delocalized charge Q_{NT} along the nanotube, and not to the local charge spot Q_{stored} left on the oxide after the WRITE step. The slope value of -0.26 is in quantitative agreement with the CNTFET electrostatic lever arm, as determined independently using a full scanning-probe method.[15] This attests that

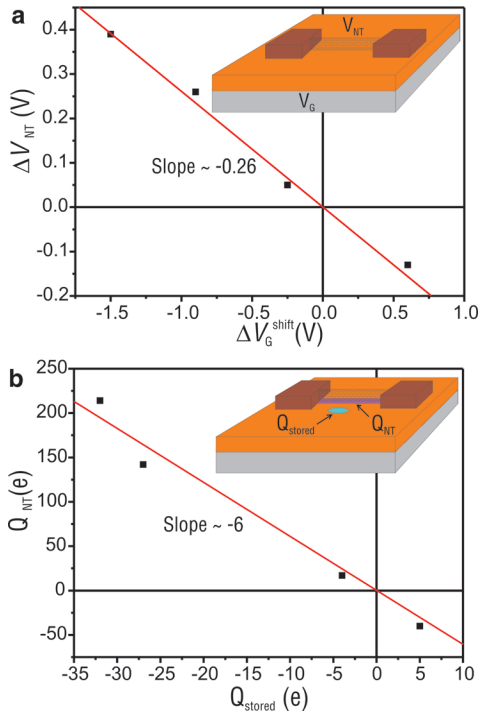

Figure 4. Device gate voltage shifts and charging. (a) Plot of the device gate voltage shift $\Delta V_{G,shift}$ as a function of the nanotube electrostatic potential shift ΔV_{NT}. The red line is a linear fit, with a −0.26 slope corresponding to the CNTFET electrostatic lever arm. (b) Plot of the charge Q_{NT} delocalized along the nanotube as a function of the charge Q_{stored} left on the oxide after the charge injection process (NVME WRITE step). The red line is a linear fit with slope −6.0 (see text).

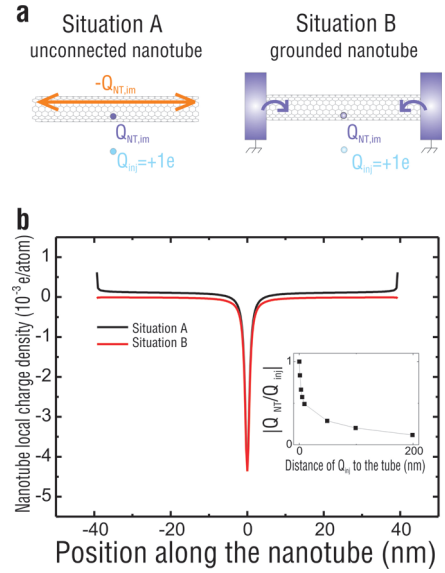

Figure 5. Atomistic electrostatic simulations. (a) (Left, situation A) Schematics of the charge distribution for an unconnected (neutral) nanotube subjected to a local charge perturbation Q_{inj}, consisting in a localized nanotube image charge $Q_{NT,im}$ and a delocalized charge $-Q_{NT,im}$ (see text). (Right, situation B) Schematics of the charge distribution for a nanotube kept at ground while subjected to a local charge perturbation Q_{inj}, and consisting only in a localized nanotube image charge $Q_{NT,im}$ imported from the nanotube leads. (b) Atomistic electrostatic simulations conducted in the dipole-charge formalism for an 80 nm long (5,5) nanotube subjected to a charge perturbation $Q_{inj} = +1e$ located 1 nm away from the nanotube middle. The black curve (situation A) corresponds to the case of the ungrounded nanotube, for which a local image charge $Q_{NT,im}$ (here equal to $-0.83Q_{inj}$) builds up in the nanotube and a delocalized charge $-Q_{NT,im}$ sets in along the nanotube to ensure its neutrality. The red curve (situation B) corresponds to the case of the grounded nanotube, in which the local image charge $Q_{NT,im}$ has been imported from the nanotube leads. Inset: dependence of the normalized nanotube image charge $|Q_{NT,im}/Q_{inj}|$ with respect to the distance of Q_{inj} to the nanotube (here calculated for a metal cylinder).

the CNTFET electrostatics has been quantitatively assessed from KFM measurements. The value of the nanotube delocalized charge Q_{NT} is then extracted from ΔV_{NT} using a cylinder-plane capacitive model, and plotted in Figure 4b as a function of the residual charge Q_{stored} left on the oxide after the local WRITE step. The linear behavior in Figure 4b with slope −6 confirms that the local charge spot Q_{stored} is only a fraction, $\alpha < 1$, of the total charge Q_{inj} which has gated the nanotube during the charge injection experiment. This point can be observed directly in the EFM image of Figure 3d in which the contrast associated with the delocalized nanotube charge Q_{NT} exceeds Q_{stored}.

To understand the operation of this NVME, we propose the following model. The tip biased at V_{inj} during the local charge injection corresponds to a charge perturbation Q_{inj} for the CNTFET, with $Q_{inj} \gg Q_{stored}$, as discussed above. In a simple view, the charge Q_{inj} will generate a local nanotube image charge $Q_{NT,im}$, of opposite sign as compared to Q_{inj}. Since the CNTFET is grounded during the injection process ($V_D = V_S = 0$), the nanotube imports from its leads a charge $Q_{NT} = Q_{NT,im}$ to keep the nanotube potential constant. After the injection process, since only $Q_{stored} \ll Q_{inj}$ is left on the SiO_2 surface (as imaged in Figure 3), the nanotube charge Q_{NT} mostly behaves as an out-of-equilibrium nanotube charge. We assume that this charge is then emitted in a delocalized way into the oxide along the nanotube, as in the case of direct local charge injection experiments into nanotubes.[14] The NVME then becomes mostly sensitive to Q_{NT} during the READ step. This simple picture accounts for both (i) the delocalized charge pattern observed in the nanotube environment after the NVME operation (Figure 3) and (ii) the NVME inverse gating as observed from its transport characteristics in Figure 2. It therefore fully corresponds to our experimental observations.

To understand the behavior of the NVME on a microscopic basis, we performed atomistic simulations of the response of the nanotube upon a local charge injection in the framework of the charge-dipole formalism.[19] This model is based on the representation of the carbon atoms by net electric charges and dipoles, which are determined from the minimization of the electrochemical energy of the system. In this context, it is the self-energy of the atomic charges that limits their ability to accumulate along the nanotube (the self-energy accounts for the repulsion between charges situated on

the same atomic site). We present in Figure 5 the results of a (5,5) nanotube[20] of total length 80 nm, subjected to a charge perturbation of $Q_{inj} = +1e$ located 1 nm away from the nanotube. The observed electrostatic behavior (see hereafter) will be extrapolated to the regime of μm -long nanotubes used in experiments. The black curve in Figure 4 (situation A) shows the charge distribution along the unconnected (neutral) nanotube upon the $Q_{inj} = +1e$ perturbation. A local (here, negative) image charge $Q_{NT,im} \simeq -0.83e$ builds up at midtube, which is compensated by an almost constant (here, positive) delocalized charge distribution $-Q_{NT,im}$ along the nanotube, accounting for the nanotube global neutrality. The charge enhancement seen at the nanotube ends originates from Coulomb interactions and is known to vanish for longer nanotubes.[21] The charge distribution is then investigated while the nanotube is grounded (red curve in Figure 4, situation B) during charge injection. The nanotube is seen to acquire a net charge $Q_{NT} = Q_{NT,im} \simeq -0.83e$, while the constant charge distribution along the nanotube has disappeared: it has, in fact, been compensated by the net charge imported from the leads. The charging process can thus be globally viewed as a transfer of the nanotube image charge $Q_{NT} = Q_{NT,im}$ from its leads, in order to keep the nanotube at ground while subjected to the local perturbation Q_{inj} during the WRITE step. This picture deduced from atomistic simulations accounts for the experimental results in Figures 2 and 3.

These calculations offer a most simple view of the charge detection efficiency in carbon nanotube devices, in which the nanotube electrostatic potential shift can be computed from the nanotube image charges, when redistributed along the nanotube length. Indeed, the situation B of the grounded nanotube corresponds to the NMVE operation of the CNTFET, as described in the present letter. A gating effect occurs, in which the nanotube electrostatic potential shift ΔV_{NT} exactly corresponds to the nanotube image charge $Q_{NT,im}$ delocalized over nanotube length. Situation A of the neutral nanotube response corresponds on the other hand to operating CNTFETs used as charge detectors,[4−7] assuming no charge accumulation in the CNTFET channel. The charge sensing comes in this situation from an electrostatic shift of the CNTFET channel ΔV_{NT}, due to the redistribution of the opposite image charge $-Q_{NT,im}$ over the nanotube length. The two situations are therefore similar in their principle, although opposite in terms of the CNTFET gate voltage shift. The simple picture based on a redistribution of the nanotube image charges along the device length also compares quantitatively with experimental data. In the case of our NVME (situation B), the nanotube image charge $Q_{NT} = -40e$ in the experiment of Figure 3 corresponds to a charge perturbation $Q_{inj} \simeq +220e$ taking into account the dependence of image charges with respect to the distance to the nanotube (see Figure 5, inset). This value corresponds to the charge $CV_{inj} \simeq 210e$ expected at the scanning-probe tip when biased as V_{inj} with the backgate, using a tip−backgate capacitance $C = 2\pi\varepsilon_0\varepsilon_{ox}R$ ($\varepsilon_{ox} = 4$, being the silicon dioxide relative dielectric constant, and $R = 25$ nm, the tip radius) and $V_{inj} = +6$ V, although an exact comparison would require a description of the full tip−nanotube−substrate geometry. Conversely, in the case of charge detectors based on CNTFETs (situation A), our model based on the redistribution of image charges can be used to estimate the CNTFET electrostatic potential shift ΔV_{NT} associated with the detection of a single charge located at a few nanometers from the device channel.[4−7] For a CNTFET of channel length 0.6 μm on a 1 μm thick SiO_2 layer (nanotube−substrate capacitance of 9 aF),[5] this predicts a nanotube electrostatic potential shift $\Delta V_{NT} \simeq 10-20$ mV for a single charge located less than 10 nm from the nanotube. This quantity is amplified by the CNTFET electrostatic lever arm when the device is operated by its backgate. It is thus consistent with the observed device backgate voltage shifts of $\Delta V_{G,shift} \simeq 60$ mV upon single-electron detection.[5]

Our experiments also bring a new insight on the nature of the CNTFET hysteresis, due to the fact that the charge perturbation occurs in the plane of the device, and is not "vertically" induced, such as in NVMEs operated in a vertical geometry.[8,9] Our geometry with a charge perturbation in the plane of the device excludes that the change of the nanotube electrostatic environment (as seen from EFM or KFM images in Figure 3) would be due to a dipolar effect, because it would then correspond to an *in-plane* dipole, which would not be visible in the scanning-probe images. The situation of Figure 2, in which the device gate voltage shift $\Delta V_{G,shift}$ can even exceed the hysteresis loop width, therefore demonstrates that the charge stored at the nanotube/SiO_2 interface does not significantly alter the width of the CNTFET hysteresis. This constitutes an important experimental piece of information with respect to the origin of hysteresis in CNTFET devices. Two explanations have indeed been referred to in literature for the hysteresis in CNTFETs: (i) the reconfiguration of mobile charges at the nanotube/dielectric interface (see, *e.g.*, refs 8 and 22) and (ii) the presence of water molecules adsorbed on the surface of the carbon nanotube itself[11] leading to hysteresis loops even for CNTFETs built on hydrophobic substrates.[23] In our experiments, since the charge density at the nanotube/SiO_2 interface has been manipulated using $\Delta V_{G,shift}$ potentials much smaller than the CNTFET transfer characteristics sweep widths (typically 7−8 V), such charges would be likely to be detrapped upon backgate voltage sweeps, if participating to the CNTFET hysteresis. The observation of mainly unchanged CNTFET hysteresis loops therefore clearly favors dipolar effects based on molecular species in the nanotube environment.

CONCLUSIONS

We have investigated the fundamental operation mechanisms of locally gated CNTFET-based NVMEs using combined transport, scanning probe techniques, and atomistic simulations. NVMEs with unchanged hysteresis have been demonstrated, in which the information is stored as a delocalized charge along the CNTFET channel. The charge storage mechanism has been attributed to the redistribution of the nanotube image charge along the device channel. This brings a most simple model for charge sensing based on CNTFETs, which could also be extended for, for example, gas sensing or biosensing. The observation of devices with unchanged CNTFET hysteresis loops underlines additionally that the hysteresis stems from dipolar effects based on molecular species in the nanotube environment, rather than on charges at the nanotube/SiO_2 interface.

EXPERIMENTAL METHODS

CNTFET devices have been achieved by depositing single-walled carbon nanotubes (Nanocyl, Belgium) onto a 320 nm-thick silicon dioxide surface thermally grown from a p-type degenerately doped silicon wafer. The deposited nanotubes (or bundles) are first localized using atomic force microscopy (in which their diameter is found between 1 and 3.3 nm). Electron beam lithography is then used to pattern the device source and drain contacts, which are finally metallized with a 20 nm-thick palladium layer.

Electrical measurements have been recorded using an Agilent 4155 semiconductor parameter analyzer. The CNTFET transfer characteristics and hysteresis measurements are achieved from backgate bias sweeps (hold time and delay time of 100 ms), starting from 0 V toward negative gate bias, then toward positive bias and finally coming back to 0 V. This sequence is repeated five times. The hysteresis data shown here correspond to an average over the last four sweeps.

Scanning probe experiments (atomic force microscopy, EFM, and KFM) have been performed with a Dimension D3100 microscope equipped with a Nanoscope IV electronics (Veeco Instruments). The microscope head and the CNTFET devices have been placed under dry nitrogen atmosphere prior to experimental data acquisition (humidity $<10\%$). All measurements have been performed using standard EFM-type tips (EFM-PPP, Nanosensors) with resonance frequency $f_0 = 70$ kHz and spring constant $= 1-3\ \mathrm{N\cdot m^{-1}}$. Topography images have been acquired in tapping mode (20 nm tip oscillation amplitude) while EFM and KFM data have been obtained in a lift mode, in which the tip is passed at a 70−80 nm distance above the sample surface topography to discard short-range surface forces and only record the effect of electrostatic forces.

EFM images are acquired by maintaining a cantilever mechanical excitation and adding a static tip detection voltage V_{EFM} (see Figure 1). They consist in mapping the shift Δf of the cantilever resonance frequency f_0, which is proportional to local electrostatic force gradients. Dark (respectively bright) features in EFM images correspond to attractive (respectively, repulsive) force gradients (as compared to the substrate), which stem from local charges and/or local changes in the tip−substrate capacitances.

KFM images consist in measuring the local surface potential V_S. They are acquired with an electrostatic excitation, using a tip voltage $V_{dc} + V_{ac}\cos(\omega t)$ (here with $V_{ac} = 2$ V) with ω close to $2\pi f_0$. This electrostatic excitation induces a force proportional to $(V_{dc} - V_S)$ at the angular frequency ω, which is set to zero using a feedback loop to nullify the cantilever oscillation at ω. This procedure enables the measurement $V_{dc} = V_S$, and thus, the mapping of local surface potentials.

To create local charge spots on the silicon dioxide surface, charge injection experiments have been used, in which the atomic force microscopy tip is pressed with a static force of a few nN on the surface (cantilever vertical deflection of a few nm), and biased using an injection voltage V_{inj} with respect to the sample backgate. This method is known to generate local spots of a few charges up to a few hundreds of charges stored at the surface oxide traps.

Acknowledgment. This work was done in the framework of the CNRS GDR-E Grant No. 2756 and supported in part by an ANR Grant No. 06-NANO-070. A.M. is funded by the National Fund for Scientific Research (FNRS) of Belgium and acknowledges the use of the Interuniversity Scientific Computing Facility (ISCF) of Namur. We acknowledge fruitful discussions with V. Derycke, M. Zdrojek, H. Diesinger, D. Deresmes, and the technical staff involved in the device processing.

Supporting Information Available: Experimental data. This material is available free of charge *via* the Internet at http://pubs.acs.org.

REFERENCES AND NOTES

1. Avouris, P.; Chen, Z. H. Perebeinos, Carbon-based Electronics. *Nat. Nanotechnol.* **2006**, *2*, 605–615.
2. Ganguly, U.; Kan, E. C.; Zhang, Y. Carbon Nanotube-Based Nonvolatile Memory with Charge Storage in Metal Nanocrystals. *Appl. Phys. Lett.* **2005**, *87*, 043108.
3. Hou, T.-H.; Raza, H.; Afshari, K.; Ruebusch, D. J.; Kan, E. C. Nonvolatile Memory with Molecule-Engineered Tunneling Barriers. *Appl. Phys. Lett.* **2008**, *92*, 153109.
4. Marty, L.; Bonnot, A. M.; Bonhomme, A.; Iaia, A.; Naud, C.; André, E.; Bouchiat, V. Self-Assembly of Carbon Nanotube Based Single Electron Memories. *Small* **2006**, *1*, 110–115.
5. Gruneis, A.; Esplaniu, M. J.; Garcia-Sanchez, D.; Bachtold, A. Detecting Individual Electrons Using Carbon Nanotube Field-Effect Transistor. *Nano Lett.* **2007**, *7*, 3766–3769.
6. Heller, I.; Janssens, A. M.; Mannik, J.; Minot, E. D.; Lemay, S. G.; Dekker, C. Identifying the Mechanism of Biosensing with Carbon Nanotube Transistors. *Nano Lett.* **2008**, *8*, 591–595.
7. Zdrojek, M.; Esplandiu, M. J.; Barreiro, A.; Bachtold, A. Electron Counting Spectroscopy of CdSe Quantum Dots. *Phys. Rev. Lett.* **2009**, *102*, 226804.
8. Fuhrer, M. S.; Kim, B. M.; Dürkop, T.; Brintlinger, T. High-Mobility Nanotube Transistor Memory. *Nano Lett.* **2002**, *2*, 755–759.
9. Radosavljevic, M.; Freitag, M.; Thadani, K. V.; Johnson, A. T. Nonvolatile Molecular Memory Elements Based on Ambipolar Nanotube Field Effect Transistors. *Nano Lett.* **2002**, *9*, 921–925.
10. Fu, W.; Xu, Z.; Bai, X.; Gu, C.; Wang, E. Intrinsic Memory Function of Carbon Nanotube-Based Ferroelectric Field-Effect Transistor. *Nano Lett.* **2009**, *9*, 921–925.
11. Kim, W.; Javey, A.; Vermesh, O.; Wang, Q.; Li, Y.; Dai, H. Hysteresis Caused by Water Molecules in Carbon Nanotube Field Effect Transistors. *Nano Lett.* **2003**, *3*, 193–198.
12. Robert-Peillard, A.; Rotkin, S. V. Modeling Hysteresis Phenomena in Nanotube Field-Effect Transistors. *IEEE Trans. Nanotechnol.* **2005**, *4*, 284–288.
13. Lee, J. S.; Ryu, S.; Kwonjae, Y.; Choi, I. S.; Yun, W. S.; Kim, J. Origin of Gate Hysteresis in Carbon Nanotube Field Effect Transistors. *J. Phys. Chem. C* **2007**, *111*, 12504–12507.
14. Zdrojek, M.; Heim, T.; Brunel, D.; Mayer, A.; Mélin, T. Inner-Shell Charging of Multiwalled Carbon Nanotubes. *Phys. Rev. B* **2008**, *77*, 033404.
15. Brunel, D.; Deresmes, D.; Mélin, T. Determination of the Electrostatic Lever Arm of Carbon Nanotube Field Effect

Transistors by Kelvin Probe Microscopy. *Appl. Phys. Lett.* **2009**, *94*, 223508.
16. Schaadt, D. M.; Yu, E. T.; Sankar, S.; Berkowitz, A. E. Charge Storage in Co Nanoclusters Embedded in SiO_2 by Scanning Force Microscopy. *Appl. Phys. Lett.* **1999**, *74*, 472.
17. Jacobs, H. O.; Leuchtmann, P; Homan, O. J.; Stemmer, A. Resolution and Contrast in Kelvin Probe Force Microscopy. *J. Appl. Phys.* **1998**, *84*, 1168.
18. In the second NVME (channel length 3.1 μm), charge injections have been conducted with $V_{inj} = -6$ V at a distance $\simeq$ 170 nm from the nanotube, in the vicinity of the device source and drain contacts. The larger values Q_{stored} of the local charge stored at the oxide surface after charge stems from an increase of the scanning-probe tip capacitance with respect to the substrate, source, and drains.
19. Mayer, A. Formulation in Terms of Normalized Propagators of a Charge-Dipole Model Enabling the Calculation of the Polarization Properties of Fullerenes and Carbon Nanotubes. *Phys. Rev. B* **2007**, *75*, 045407.
20. The semiconducting or metallic properties of the nanotube is not relevant as is its transverse dielectric properties, see for example: Kozinsky, B.; Marzari, N. Dielectric Properties of Carbon Nanotubes from First Principles. *Phys. Rev. Lett.* **2006**, *96*, 166801. A metallic (5,5) nanotube is here chosen to describe its charging properties in the framework of the charge-dipole model.
21. Wang, Z.; Zdrojek, M.; Mélin, T.; Devel, M. Electric Charge Enhancements in Carbon Nanotubes: Theory and Experiments. *Phys. Rev. B* **2008**, *78*, 085425.
22. Bradley, K.; Cumings, J.; Star, A.; Gabriel, J. C. P.; Grüner, G. Influence of Mobile Ions on Nanotube Based FET Devices. *Nano Lett.* **2003**, *3*, 639–641.
23. Aguirre, C. M.; Levesque, P. M.; Paillet, M.; Lapointe, F.; St-Antoine, B. C.; Desjardins, P.; Martel, R. The Role of the Oxygen/Water Redox Couple in Suppressing Electron Conduction in Field-Effect Transistors. *Adv. Mater.* **2009**, *21*, 3087–3091.